JOURNAL OF Applied Polymer SCIENCE

Thermal and mechanical properties of PA12/C30B nanocomposites in relationship with nanostructure

Hanaya Hassan,[1] Nourredine Aït Hocine,[2] Pascal Médéric,[3] Marie-Pierre Deffarges,[4] Nathalie Poirot[5]

[1]LMR, Université François Rabelais de Tours, 7 avenue Marcel Dassault, 37200 Tours, France
[2]LMR, INSA Centre Val de Loire, 3 rue de la chocolaterie, BP 3410, 41034 Blois, France
[3]LIMATB, Equipe de Rhéologie, UBO, 6 Avenue Le Gorgeu, C.S. 93837, 29238 Brest Cedex 3, France
[4]CERMEL, Université François Rabelais de Tours, 29 rue des Martyrs, 37300 Joué-Lès-Tours, France
[5]GREMAN, IUT de Blois, 15 rue de la chocolaterie, 41000 Blois, France
Correspondence to: N. Aït Hocine (E-mail: nourredine.aithocine@insa-cvl.fr)

ABSTRACT: This work focuses on the effect of nanoclay mass fraction on the properties of polyamide 12 matrix. Relationships between mechanical, thermal, and structural properties of polyamide 12/Cloisite® 30B nanocomposites were studied. The material structure, previously described from XRD and TEM experiments, was more thoroughly characterized in the present work using SEM and FTIR techniques. The FTIR results clearly showed that clay galleries are intercalated by PA chains, which leads to a partially exfoliated nanostructure, confirming the TEM observations and the XRD analysis. However, a few micrometric aggregates are evidenced by SEM analysis, particularly at high clay fractions. TGA and DTA measurements showed that the thermal stability of PA12 matrix is slightly modified by the Cloisite® 30B content. Viscoelastic properties of the nanocomposites in solid-state were analyzed as functions of strain, frequency, and temperature. The extent of the linear response regime of the material is shown to be sensitive to the amount of clay: nonlinearities appear at lower strain values as the clay mass fraction increases. Both relative dynamical moduli also increase with increasing clay mass fraction, with frequency dependence for the viscous modulus and without frequency dependence for the elastic modulus. Finally, similarities have been pointed out between viscoelastic properties of the nanocomposites in solid and melt states. For example, the percolation threshold is highlighted at the same clay mass fraction, ~2%, in both states. © 2015 Wiley Periodicals, Inc. J. Appl. Polym. Sci. **2015**, *132*, 41938.

KEYWORDS: clay; mechanical properties; nanostructured polymers; polyamides; thermal properties

Received 15 September 2014; accepted 24 December 2014
DOI: 10.1002/app.41938

INTRODUCTION

Over the past two decades, big efforts have been devoted to study polymer/lamellar clay nanocomposites because of their improved properties as compared to those of the neat polymers or conventional microcomposites. Main developments in terms of processing and characterization of polymer/layered silicate nanocomposites have been reported by two reviews.[1,2] Organically modified montmorillonite (OMMT) is the most commonly used layered silicate. Indeed, obtaining the nanoscale structure requires a cationic exchange that usually consists in replacing metal cations present in montmorillonite galleries by quaternary alkyl ammonium cations. In that case, nanocomposites exhibit significant improvements in properties, such as mechanical performances, gas permeability, thermal stability, and flame retardancy.[1–7] These improvements obtained at very low nanofiller contents preserve the good processability of polymers. They depend on several factors: size and aspect ratio of filler, degree of dispersion, and orientation of nanoparticles within the matrix, as well as interaction between filler and polymer matrix.

According to the literature,[8] organically modified montmorillonite can be efficiently exfoliated in polar matrices using appropriate mixing conditions.[9,10] Therefore, among all polymer/layered silicate nanocomposites of potential commercial interest, particular attention was paid to nanocomposites based on polyamides: polyamide 6 (PA6),[10–13] polyamide 11 (PA11),[13] and polyamide 12 (PA12).[9,13–18] The low melting point of the polyamide 12, compared to other polyamides, successfully allows the elaboration of nanocomposites and reduces the thermal degradation of alkyl quaternary ammonium ions beginning generally at 180°C.[19] This degradation is due to, among others, high mixing temperature or/and high mixing mechanical energy, and can lead to nanocomposites based on OMMT with poor macroscopic properties, such as mechanical[15] and

rheological[18] properties, whichever the kind of the matrix used. However, under appropriate processing conditions, it was shown that the PA12/layered silicate nanocomposites have interesting performances.[14] More precisely, the linear and nonlinear mechanical properties of PA12/OMMT nanocomposites determined from tensile tests, have highlighted the existence of a OMMT mass fraction threshold at ~2%,[17] identified with a percolation threshold from the study of relationships between structure and melt-state rheological properties of these systems.[16]

This paper studies the influence of nanoclay mass fraction on structural, thermal, and dynamical mechanical properties of PA12/OMMT nanocomposites. In particular, viscoelastic properties of solid nanocomposites were evaluated with a dynamical mechanical thermal analyzer (DMTA), using strain sweep, frequency sweep, and temperature sweep experiments. To the best of our knowledge, the large panel of DMTA tests proposed in this study, which has never been thoroughly investigated in the literature, is an original work. In fact, in the published papers, only temperature sweep experiment was commonly used,[20] generally to determine the glass transition temperature of materials.[21] The aim of this paper is to study the relationships between structure and macroscopic properties of PA12/C30B nanocomposites. Moreover, a comparative study between viscoelastic parameters of the studied materials in solid-state and melt-state was also conducted, which represents another originality of this work.

EXPERIMENTAL

Materials

The polymer used as a matrix in this work is a polyamide 12 (PA12), referenced as Rilsan® AECHVO and supplied by the ARKEMA group (Serquigny, France). The molecular characteristics of this commercial polymer have been characterized by Talon.[22] The number average molar mass was shown to be 20,000 g/mol and the polydispersity index was found to be 1.9. The melting point of this PA12 grade is 183°C.

The silicate used to reinforce the matrix is an organically modified montmorillonite clay, named Cloisite® 30B (C30B), and supplied by Southern Clay Products (Gonzales). From supplier data, C30B is methyl tallow *bis*-2-hydroxyethyl ammonium exchanged montmorillonite clay with a cationic modifier concentration of 90 milliequivalents per 100 g. The density of this organophilic clay is 1.98.

Nanocomposite Elaboration

Although the PA12 has a weak hygroscopic character,[23] it was first dried at 80°C for 4 h in vacuum before nanocomposite preparation. Nanocomposites were prepared by melt intercalation in a Haake Rheocord internal mixer, under nitrogen atmosphere. The two components were mixed at a blade rotation speed of 100 rpm for 6 min. To minimize the degradation of the composite components during mixing, particularly the alkyl ammonium ions, the processing temperature was fixed at 200°C, which corresponds to 20°C above the melting point of PA12.

Samples were pelletized and processed by compression molding at 200°C between 2 mm thick plates, at several clay mass fractions ranging from 0 to 10 wt %.

Nanocomposite Structure

The structure of PA12/C30B materials was characterized by X-ray diffraction (XRD) and transmission electron microscopy (TEM) techniques in previous works.[9,16,18] It was proved that the structure is partially exfoliated/intercalated. Moreover, the specific particle density D, as defined by Fornes *et al.*[24] in order to quantify the degree of exfoliation, was measured from TEM micrographs and was found to decrease with increasing clay mass fraction.

In this work, the structure analysis of the PA12/C30B nanocomposites is completed by scanning electron microscopy (SEM) observations, carried out with a ZEISS ULTRA Plus field emission apparatus operating at 5 kV. Beforehand, samples were cut into 1 mm thick pieces and embedded into an Epon-type epoxy resin (polymerized at 60°C for 48 h).

At last, physical–chemical characterizations of PA12, C30B, and all PA12/C30B nanocomposites were conducted with transmission mode Fourier-transformed infrared (FTIR) spectroscopy. The spectra were measured using a Perkin-Elmer Spectrum One FTIR ATR, in the wave frequencies ranging from 400 to 4000 cm^{-1}, with a resolution of 4 cm^{-1} and using 25 scans.

Nanocomposite Characterizations

Thermogravimetric analyses (TGA) were performed using a Perkin Elmer TGA 7. The samples of about 12 mg were heated from room temperature up to 800°C, at a rate of 10°C/min and under a nitrogen atmosphere. The mass variation of samples was gradually measured during the degradation of the material. These analyses should allow the determination of the clay mass fraction actually present in each nanocomposite and to give information about the influence of clay content on the nanocomposite thermal stability.

Differential thermal analyses (DTA) were conducted on a Perkin-Elmer DTA-7 in a nitrogen environment. The samples of about 10 mg were heated from room temperature up to 250°C, at a rate of 10°C/min and then were held at 250°C for 10 min in order to eliminate the influence of thermal history. Finally, they were cooled from 250 to 25°C at a rate of 10°C/min. This heating–cooling cycle was twice achieved on the same specimen.

Rectangular specimens (16 × 4 × 2 mm^3) of PA12 matrix and nanocomposites were subjected to cyclic dynamical loadings using a dynamical mechanical thermal analysis (DMTA) machine VA4000, commercialized by 01db-Metravib society. Strain sweep tests, frequency sweep tests, and temperature sweep tests were carried out under tensile mode and the material viscoelastic properties were recorded.

During strain sweep tests, specimen were submitted to an increasing sinusoidal strain ranging from 2.10^{-4} to 7.10^{-3}, at room temperature and frequency of 1 Hz.

Frequency sweep tests were carried out in the range from 10^{-4} to 40 Hz at room temperature, under the static displacement of 10 μm and by imposing sinusoidal strain amplitude of 7.10^{-4}.

Finally, samples were submitted to temperature sweep tests in the range from −20 to 180°C with the heating rate of 3°C/min and under liquid nitrogen flow. They were scanned at a fixed

frequency of 1 Hz, under an imposed constant load of 4 N and sinusoidal strain amplitude of 7.10^{-4}.This amplitude value was selected in the linear viscoelastic domain of all the studied materials.

RESULTS AND DISCUSSION

Nanocomposite Structure

Scanning Electron Microscopy. In this work, the structure of the PA12/C30B nanocomposites[9,16–18] was observed by SEM at a micrometric scale.

Figure 1 presents the SEM micrographs of nanocomposites with 1, 5, and 10% of clay mass fractions at the same magnification. They reveal the presence of a few objects corresponding to micrometric clay aggregates. Their number and sizes clearly increase with increasing clay mass fraction, in agreement with the decrease of the specific particle density.[18] In fact, the intercalated/exfoliated nanostructure, previously characterized by TEM and XRD techniques,[9,16,18] clearly governs the macroscopic behavior of PA12/C30B composites, such as rheological properties[9,16,18] and mechanical properties at break.[17] To summarize, the structure, mainly nanometric, is accompanied with a few micrometric entities which are some potential structural defects, in particular as regard of mechanical properties at break, at high clay fractions.[17]

Fourier Transformed Infrared Spectroscopy. FTIR spectra of nanocomposites with various clay mass fractions are displayed in Figures 2 and 3. The latter is a zoom of wavelength region ranging from 900 to 1200 cm^{-1}.

In Figure 2, characteristic vibration modes of the hydroxyl group are present. In fact, its bending and stretching bands are observed at ~1640 and ~3440 cm^{-1}, respectively.[25] The peaks at 920 and 3630 cm^{-1}, commonly attributed to Al_2–OH grouping[26] and characteristic of C30B, are little marked because of the weak amount of clay present and, moreover, well dispersed in PA12 matrix.

Moreover, FTIR spectrum shows asymmetric and symmetric bending bands, at ~2850 and ~2920 cm^{-1}, respectively, and stretching band at 1470 cm^{-1} corresponding to C–H_2 bonds.[27,28] Intensities of the three peaks, characteristic of quaternary alkyl ammonium modifier, increase with C30B mass fraction. This means that the quaternary alkyl ammonium, favoring the intercalation of PA12 macromolecular chains into clay galleries, is not completely degraded after the nanocomposite mixing at 200°C.

FTIR spectra of all nanocomposites clearly show the characteristic bands of Si–O vibrations at 1020, 1040, 1075, and 1120 cm^{-1},[29–31] whose intensities significantly increase with the number of Si–O groupings, i.e., with increasing C30B mass fraction (Figure 3). The peak at 1040 cm^{-1} observed in the spectra of nanocomposites, is the signature of a partially intercalated structure of PA12/C30B nanocomposites,[23,32] also evidenced by X-ray diffraction results.[16,18]

At last, the greater distance between clay layers which is due to the exfoliation of these particles and/or to the intercalation of PA12 chains in their galleries (exfoliated/intercalated structure), could explain the weak intensity of stretching vibration mode of the C–C linkage (at 1000 cm^{-1}), which increases with clay mass fraction (Figure 3).

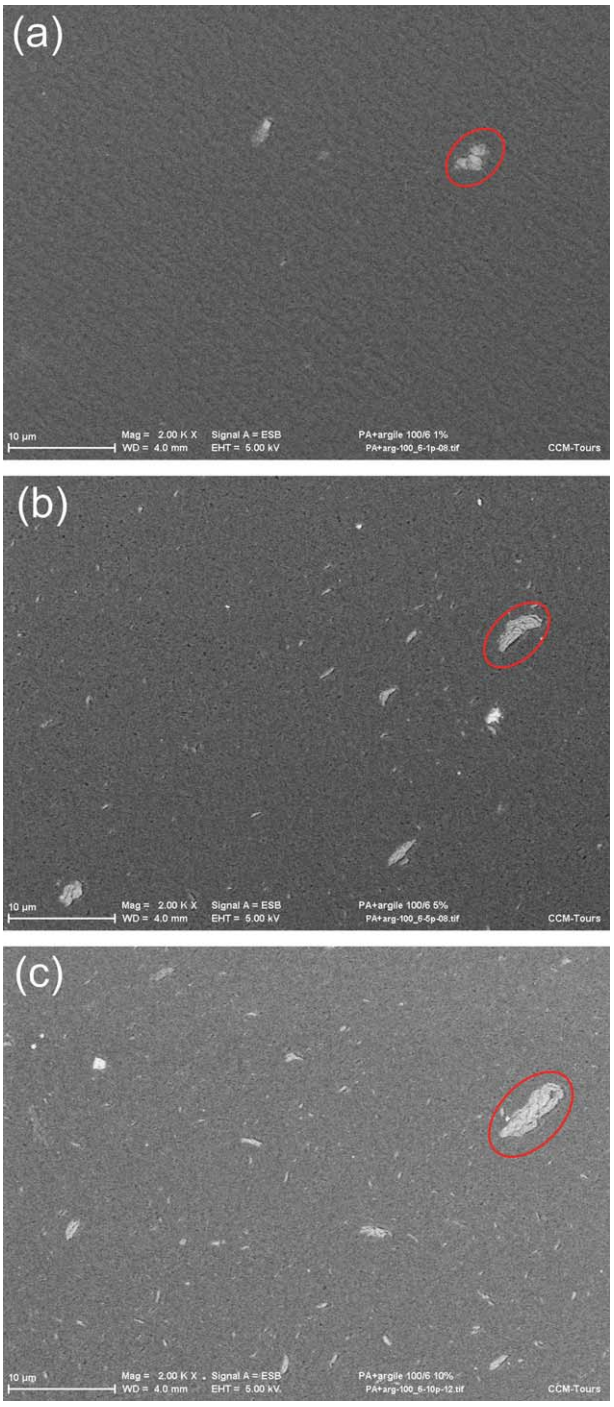

Figure 1. SEM micrographs of nanocomposites with (a) 1%, (b) 5%, and (c) 10% of C30B. [Color figure can be viewed in the online issue, which is available at wileyonlinelibrary.com.]

Thermal Properties

Thermogravimetric Analysis. Figure 4 shows the weight loss of the Cloisite® 30B as a function of temperature. The weight loss observed at 200°C is certainly due to the partial degradation of

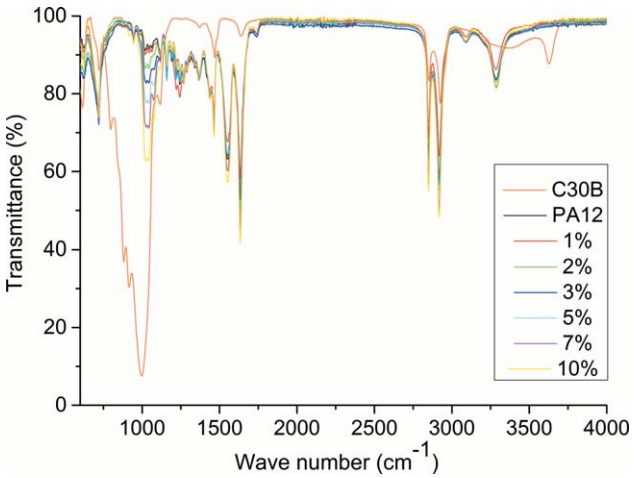

Figure 2. FTIR spectra of nanocomposites. [Color figure can be viewed in the online issue, which is available at wileyonlinelibrary.com.]

the alkyl quaternary ammonium used as organic modifier for C30B clay, as discussed by Xie *et al.*[19] The weight loss increases significantly and gradually between 200 and 450°C up to a value of 24%, attributed to the total degradation of the montmorillonite organic modifier. In fact, the first derivative of the thermogravimetric curve of Cloisite® 30B shows a pronounced degradation around 273 and 374°C (Figure 4). Another significant weight loss at 587°C is attributed to the dihydroxylation of the clay layers.[19] At 800°C, there is ~72.5% of clay mineral residue. Above all, results suggest that the mixing temperature of 200°C chosen to prepare the studied nanocomposites, avoids a pronounced degradation of the clay organic modifier.

Figure 5 presents the thermogravimetric curves of PA12 and nanocomposites with C30B mass fraction ranging from 1 to 10%. Three principal zones can be identified in these thermogravimetric curves: ambient −400, 400–500, and 500–800°C. The nanocomposite weight loss below 400°C is due to the degradation of the clay organic modifier. In fact, this loss increases with increasing clay mass fraction. For example, it is of about 2% for

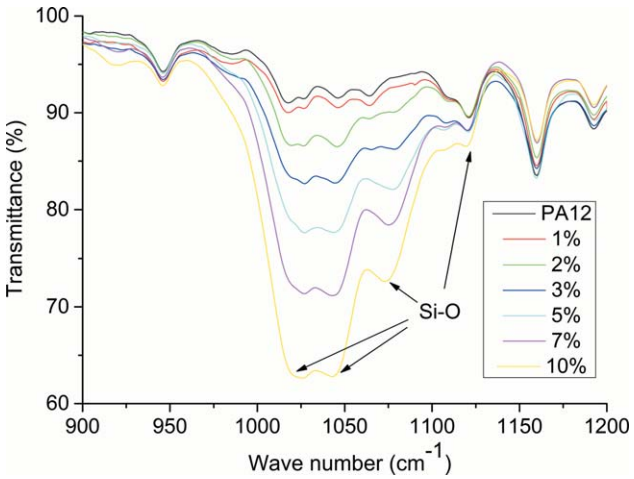

Figure 3. FTIR spectra of nanocomposites (zoom of Figure 2). [Color figure can be viewed in the online issue, which is available at wileyonlinelibrary.com.]

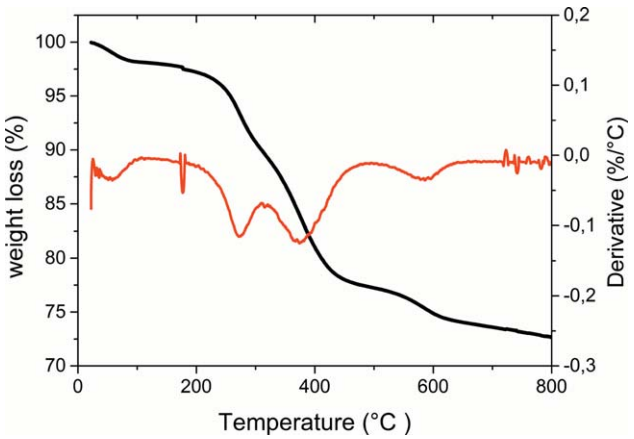

Figure 4. TGA and first derivative curves of C30B. [Color figure can be viewed in the online issue, which is available at wileyonlinelibrary.com.]

the nanocomposite with 10 wt % C30B (Figure 5), corresponding to the degradation of the alkyl quaternary ammonium, i.e. 20% of clay fraction (Figure 4). The solid mass fraction, measured at 800°C, corresponds to the clay mineral residue (Figure 5) and represents ~72.5% of the modified montmorillonite mass fraction (with the surfactant present in the composite at 200°C), called "measured clay mass fraction" and denoted ϕ_m. The values of clay mass fractions, ϕ and ϕ_m, are reported in Table I. The difference between ϕ_m and ϕ is less than 10% and is probably due to errors induced during the clay weighing and to probable losses of clay during its incorporation in the internal mixer. The measured clay mass fraction, ϕ_m, will be used as abscissa in some curves, while, for sake of clarity, the clay mass fraction, ϕ, will be used in discussions.

Finally, clay degradation is significant in the temperature range from 430 to 480°C (Figure 5). The TGA curves of PA12 matrix and nanocomposites are relatively close, indicating that clay does not notably affect the thermal stability of polyamide 12, as already suggested by several authors.[33,34] However, in order to analyze more precisely the effect of clay mass fraction on this thermal stability, the degradation starting temperature (T_s)

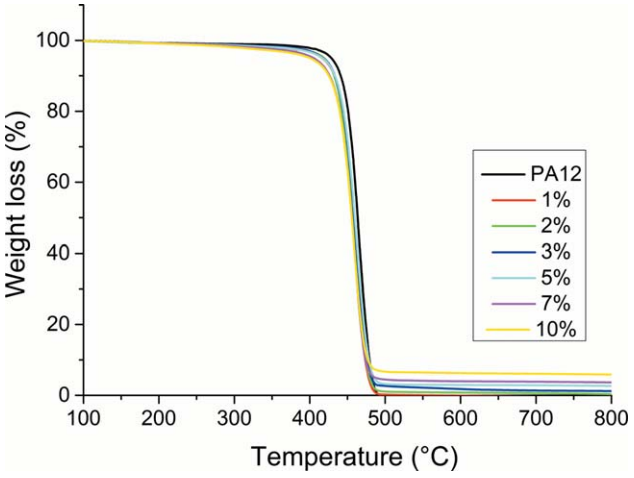

Figure 5. TGA curves of PA12 and nanocomposites. [Color figure can be viewed in the online issue, which is available at wileyonlinelibrary.com.]

Table I. Clay Mass Fractions: Introduced Mass (ϕ) and Measured Mass (ϕ_m)

ϕ (%)	ϕ_m (%)
0	0
1	1.02
2	1.80
3	2.55
5	4.80
7	7.15
10	9.20

determined by the method of tangents is presented as a function of the measured clay mass fraction ϕ_m in Figure 6. This figure exhibits two behaviors separated by a threshold value $\phi_c \sim 2\%$, already evidenced by mechanical and rheological characterizations carried out on the same materials analyzed herein.[16–18] Below the threshold value, T_s decreases with increasing clay fraction while it stabilizes beyond $\phi_c \sim 2\%$, i.e. for nanostructured composites exhibiting a percolation network.

The decrease at weak clay fractions is probably caused by the organic modifier that obviously accelerates the thermal degradation of the material. Beyond the percolation threshold, $\phi_c \sim 2\%$, this phenomenon is counterbalanced by clay network structure which plays a role of thermal barrier and stabilizes the degradation temperature at a value about 10°C lower compared to that of PA12 matrix.

Finally, Figure 7 represents the first derivative of thermogravimetric curves for the PA12 matrix and the nanocomposites with 1–10% of C30B. All curves reveal a peak near 464°C corresponding to the average temperature of material thermal degradation. The peak intensity decreases with increasing clay mass fraction, suggesting that the thermal degradation rate of nanocomposite gradually decreases as clay content increases. Indeed, the first derivative can be expressed by the following equation:

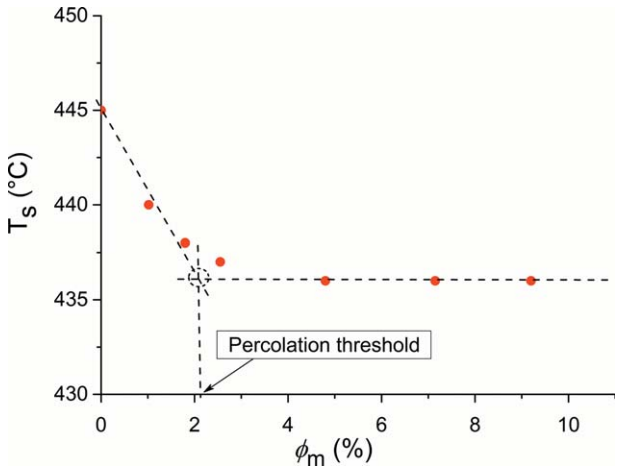

Figure 6. Degradation starting temperature T_s as a function of measured clay mass fraction. [Color figure can be viewed in the online issue, which is available at wileyonlinelibrary.com.]

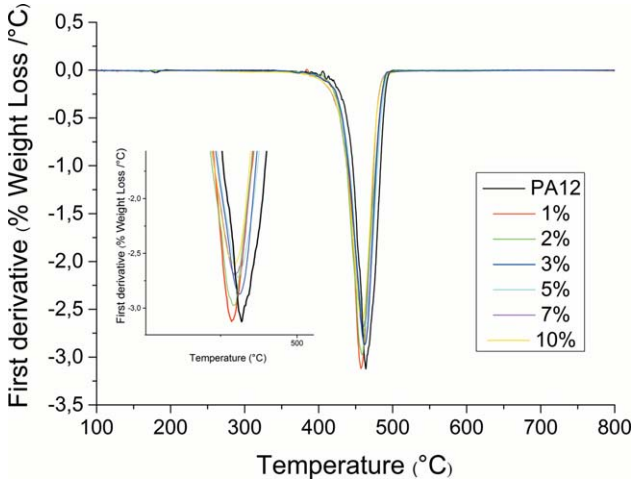

Figure 7. TGA first derivatives as functions of temperature. [Color figure can be viewed in the online issue, which is available at wileyonlinelibrary.com.]

$$\frac{dw}{dT} = \frac{dw/dt}{dT/dt}, \quad (1)$$

where w, t, and T represent the weight loss, the time and the temperature, respectively. As all TGA measurements were performed under the same heating rate dT/dt, the first derivative dw/dT is proportional to dw/dt.

Differential Thermal Analysis. The heat flow is measured as a function of temperature during the two heating–cooling cycles. These experiments are used to evaluate the glass transition peak temperature T_g, the melting peak temperature T_m, the crystallization peak temperature T_c, and the melting enthalpy ΔH_m. The degree of the crystallinity X_c is determined from the following equation:

$$X_c = \frac{\Delta H_m}{(1-0.01\phi_m)\Delta H_{m0}} \times 100 \quad (2)$$

$\Delta H_{m0} = 209.02$ J/g being the specific enthalpy at the melt-state of the 100% crystalline PA12.[15]

The two heating–cooling cycles give the same information in terms of transition temperatures. Therefore, only the first cycle is analyzed. Thus, the values of thermal properties issued from this cycle are reported in Table II and discussed as functions of clay mass fraction. For all systems, the glass transition temperature is close to 60°C and it slightly increases for

Table II. DTA Results for PA12 Matrix and Nanocomposites

Material	T_g (°C)	T_f (°C)	ΔH_m (J/g)	T_C (°C)	X_C (%)
PA12	59.7	178	34.4	158	16.4
PA + 1% C30B	59.7	177	34.3	159	16.6
PA + 2% C30B	59.7	177	34.8	158	17.0
PA + 3% C30B	59.6	177	34.8	158	17.2
PA + 5% C30B	59.7	177	34.4	157	17.3
PA + 7% C30B	60	176	33.1	156	17.0
PA + 10% C30B	60.3	176	32.2	155	17.1

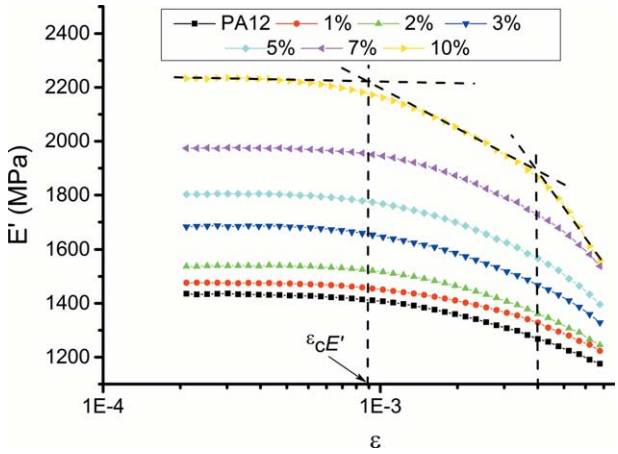

Figure 8. Storage modulus E' as a function of deformation at ambient temperature and frequency of 1 Hz. [Color figure can be viewed in the online issue, which is available at wileyonlinelibrary.com.]

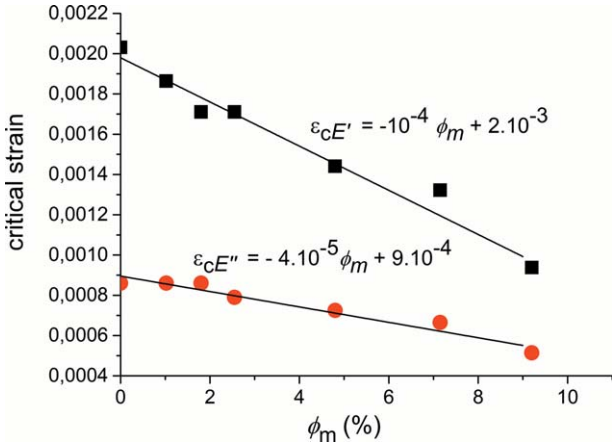

Figure 10. Critical strain as a function of measured clay mass fraction. [Color figure can be viewed in the online issue, which is available at wileyonlinelibrary.com.]

nanocomposites filled with 5% of C30B at least. This increase can be explained by the reduced mobility of PA12 chains at high clay mass fractions. On the contrary, the melting temperature of nanocomposites, ~177°C, seems independent of clay mass fraction.

The crystallinity degrees of nanocomposites are close to that of the matrix PA12 (Table II) meaning that the amount of crystallites is only little affected by the presence of clay, as reported in the literature.[35,36] Table II also shows that the crystallization temperature slightly decreases with increasing clay mass fraction, which agree with the results obtained for polyethylene terephthalate/C30B systems.[37,38] This suggests that the clay does not act as a nucleating agent for crystallization.

All these results show, in agreement with the results of the literature, that C30B clay does not considerably affect the thermal properties of PA12 matrix, particularly in the range of temperatures less than the processing temperature of nanocomposites PA12/C30B, i.e., 200°C.

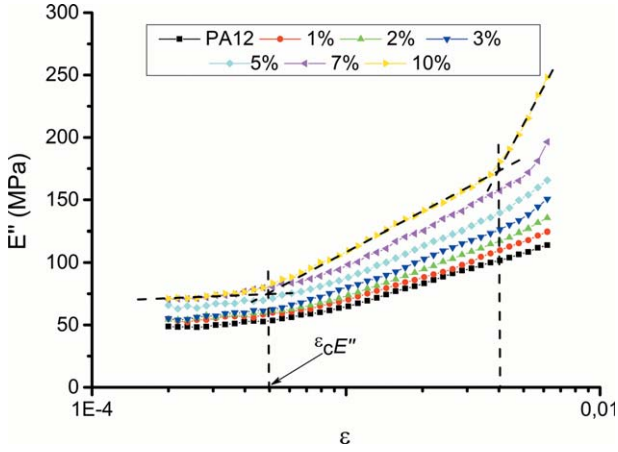

Figure 9. Loss modulus E'' as a function of deformation at ambient temperature and frequency of 1 Hz. [Color figure can be viewed in the online issue, which is available at wileyonlinelibrary.com.]

Mechanical Properties

Strain Sweep. Figures 8 and 9 present storage modulus E' and loss modulus E'' as functions of strain ε, at frequency of 1 Hz and at room temperature, for PA12 matrix and nanocomposites.

The storage modulus shows a plateau at low strains whose value increases with increasing clay fraction, from 1400 MPa for the PA12 matrix to 2200 MPa for the PA12/10% C30B nanocomposite. E'–ε curves exhibit a slope change corresponding to a critical strain denoted $\varepsilon_{cE'}$, evaluated by the method of tangents, as shown in Figure 8. The loss modulus also exhibits a plateau at low strains and its value increases from ~50 MPa for the matrix to ~70 MPa for the PA12/10% C30B nanocomposite (Figure 9). This means that the viscosity, as well as the rigidity, of nanocomposites increases with clay fraction. On the other hand, the loss modulus is less than the storage modulus in the whole range of strain studied, which proves that the contribution of the viscosity of PA12/C30B nanocomposites is lower than that of their elasticity. The loss moduli E'' of nanocomposites also highlight a slope break at a critical strain denoted $\varepsilon_{cE''}$, evaluated by the method of tangents, as shown in Figure 9. Both strains, $\varepsilon_{cE'}$ and $\varepsilon_{cE''}$ linearly decrease with increasing clay mass fraction, as shown in Figure 10, indicating that the linear behavior domain of the material becomes smaller at the expense of its nonlinear behavior domain. The critical strain $\varepsilon_{cE''}$ issued from loss modulus E'' (Figure 9) is almost twice smaller than its homolog parameter $\varepsilon_{cE'}$ issued from the storage modulus E' (Figure 8). This means that E'' is more sensitive than E' to the effects of the material behavior nonlinearities. So, for the studied materials, $\varepsilon_{cE''}$ seems to be the pertinent critical strain, indicating the limit between linear and nonlinear zone of the material behavior. It is attributed to the nonlinearities caused by the clay entities.

Moreover, for nanocomposites with $\phi > 2\%$, i.e., for structured nanocomposites having a clay percolation network, a second slope break appears at high strains in E''–ε curves (Figure 9). This change in slope, probably associated to the nonlinearities related to networked domains composed of correlated clay

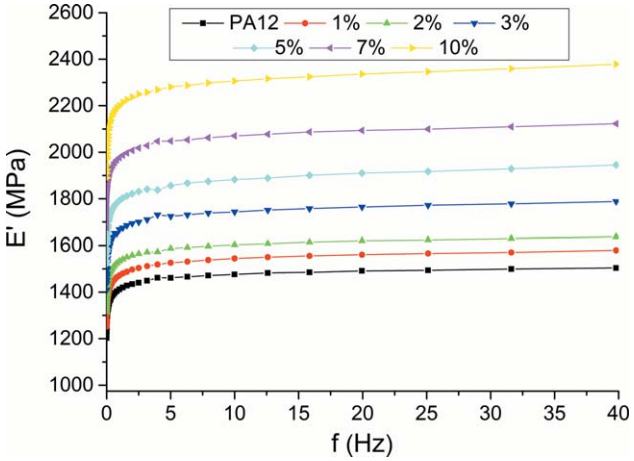

Figure 11. Storage modulus E' as function of frequency at ambient temperature and dynamical strain amplitude of 7.10^{-4}. [Color figure can be viewed in the online issue, which is available at wileyonlinelibrary.com.]

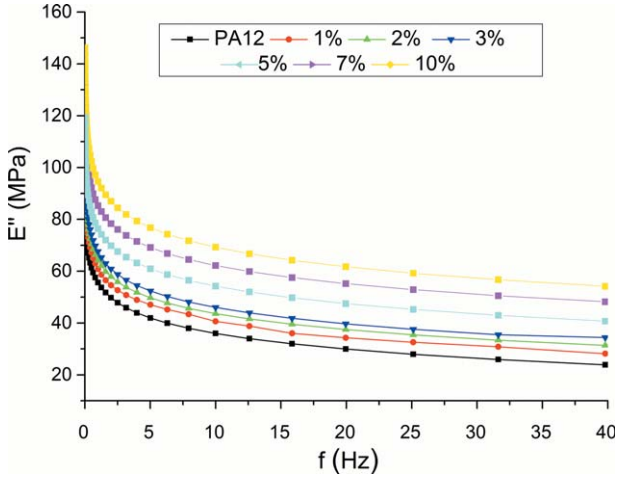

Figure 12. Loss modulus E'' as function of frequency at ambient temperature and dynamical strain amplitude of 7.10^{-4}. [Color figure can be viewed in the online issue, which is available at wileyonlinelibrary.com.]

entities evoked by Aubry *et al.*,[16] is more pronounced and occurs at smaller strains when clay mass fraction increases. This second slope break is only observable at 10% of clay in E'–ε curves. This result confirms that E'' is more sensitive than E' to the structure effects in solid-state, unlike what happens in melt-state.

Contrary to solid-state dynamical mechanical measurements, melt-state rheological measurements lead to a critical strain, γ_c, independently deduced from loss module or storage modulus. γ_c decreases with increasing clay fraction, like $\varepsilon_{cE'}$ and $\varepsilon_{cE''}$. However, this decrease, which is indicative of amplification of the nonlinear behavior induced by the presence of clay particles, is linear in the solid-state ($\varepsilon_c \sim -\phi^{+1}$) (Figure 10), whereas it is nonlinear in the melt-state ($\gamma_c \sim \phi^{-1}$).[16] This divergence can be explained by several aspects: (i) difference in the applied stress (shear in melt-state and tension in solid-state), (ii) difference in the sensitivity of measurement devices used in the melt-state and in the solid-state, and (iii) differences in filler/filler and filler/matrix interactions, partly governed by the mobility of PA12 macromolecules chains that is easier in the melt-state than in the solid-state.

Frequency Sweep. The storage and loss moduli are presented as functions of frequency in Figures 11 and 12 for PA12 matrix and nanocomposites, respectively. Figure 11 clearly shows that the storage modulus E' sharply increases at low frequencies and tends to a stabilization value beyond the frequency of about 1 Hz. Moreover, this modulus increases with increasing clay mass fraction whatever the frequency, proving the reinforcing effect of clay particles. Unlike the storage modulus E', the loss modulus E'' strongly decreases at low frequencies, as shown by Figure 12. However, like the storage modulus, the loss modulus tends to a stabilization value beyond the same frequency of ~1 Hz. At last, E'' is much lower than E' over all the range of frequencies, confirming the weak contribution of viscosity compared to that of elasticity.

The relative storage modulus E'_{relative} defined as the ratio $E'_{\text{nanocomposite}}/E'_{\text{matrix}}$ and shown in Figure 13, increases with clay fraction independently of frequency. A slope change is evidenced at a clay mass fraction of about 2%. This critical fraction, beyond which a percolation network is formed in the PA12/C30B nanocomposites, has already been highlighted by the degradation starting temperature above discussed, by melt-state rheological properties[16] as well as linear and nonlinear mechanical properties.[17] It should be noted that the increase of relative storage modulus is less significant beyond this critical clay fraction, i.e. for structured nanocomposites. This trend is predicted by analytical models, including the two-phase model[39] and the three-phase model.[40] These models were successfully applied by Aït Hocine *et al.*[17]

Figure 14 shows the relative loss modulus $E''_{\text{relative}} = E''_{\text{nanocomposite}}/E''_{\text{matrix}}$ as a function of the clay mass fraction, at different frequencies. It can be seen that E''_{relative} increases with increasing clay fraction, whatever the frequency. But, unlike the relative storage modulus that is independent of frequency for a given clay mass fraction, the relative loss modulus increases as

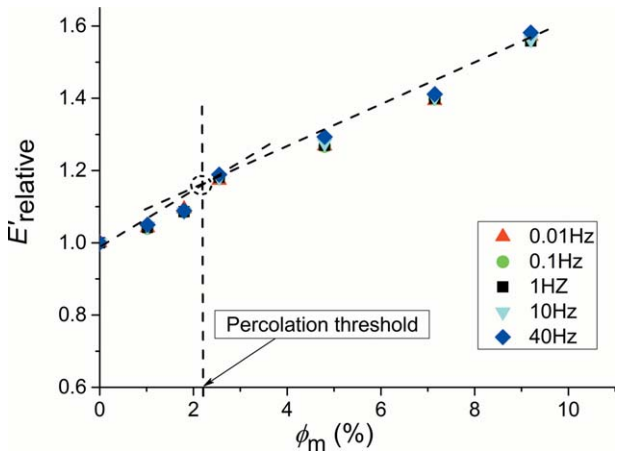

Figure 13. Relative storage modulus as a function of measured clay mass fraction at different frequencies. [Color figure can be viewed in the online issue, which is available at wileyonlinelibrary.com.]

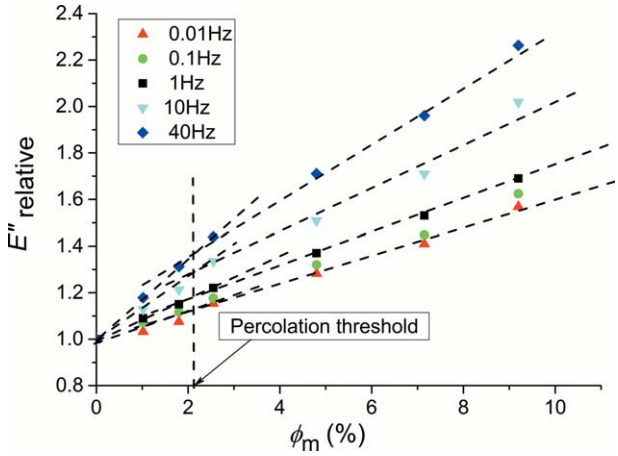

Figure 14. Relative loss modulus as a function of the measured clay mass fraction at different frequencies. [Color figure can be viewed in the online issue, which is available at wileyonlinelibrary.com.]

frequency increases, more particularly in the case of highly filled nanocomposites. Furthermore, a slope break also appears in $E''_{relative} - \phi_m$ curves at $\phi_c \sim 2\%$, regardless of the frequency (Figure 14). The increase of $E''_{relative}$ with clay fraction is also smaller beyond this threshold fraction, i.e., for the structured nanocomposites. This suggests that the relative loss modulus, like the relative storage modulus, is sensitive to the structure of nanocomposite.

It should be noted that, whatever the frequency ranging from 0.01 to 40 Hz, relative dynamical moduli measured at ambient temperature are less sensitive to clay fraction than those measured at 200°C by Aubry *et al.*[16] This can be partially explained by the difference in stiffness between the matrix and the particles, that is more high in the case of the melt-state.

Temperature Sweep. Figure 15 shows the storage modulus E' and the damping factor tan δ versus temperature, for PA12 matrix and nanocomposites with 1, 5, and 10% of C30B clay.

Storage modulus decreases with increasing temperature, which is an usual behavior of thermoplastic polymers, induced by the

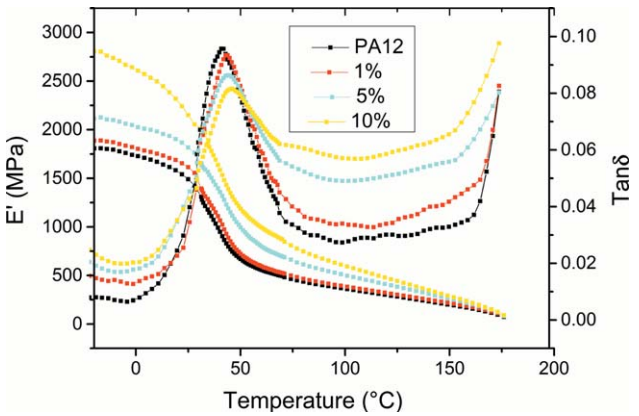

Figure 15. Storage modulus E' and damping factor tan δ as functions of temperature at frequency of 1 Hz and dynamical strain amplitude of 7.10^{-4}. [Color figure can be viewed in the online issue, which is available at wileyonlinelibrary.com.]

Table III. Storage Modulus E', Damping Factor tan^{TM}, and Glass Transition Temperature Tg of PA12 Matrix and Nanocomposites

ϕ (%)	ϕ_m (%)	E' at −20°C	E' at 100°C	tan δ	T_g
0	0	1810	360	0.096	44
1	1.02	1890	385	0.094	46
5	4.80	2115	500	0.087	46
10	9.20	2810	595	0.081	48

movement facility of macromolecular chains as the temperature increases. The modulus E' sharply falls between 35 and 75°C. This drop is accompanied by a very marked peak in the curve of tan δ, which is a signature of the material glass transition temperature, T_g. The storage modulus E' increases with increasing clay mass fraction, regardless of the glassy or rubbery zone of the material, highlighting the reinforcement role played by clay fillers (Table III). This reinforcement seems to be slightly stronger in rubber domain than in glassy domain. It should be noted that the curves become closer near the temperature of 180°C corresponding to the melting temperature of the PA12 matrix and all the studied nanocomposites.

The glass transition temperature, associated with the peak maximum of *tanδ*, is ∼44°C for PA12. It is slightly superior to the measure given by DSC (∼40°C),[41] which agrees with the results reported by Corcione *et al.*[20] but it is significantly lower than that measured by DTA (∼60°C). This difference is probably due to the fact that the heating rate selected in DMTA tests is smaller than that adopted in DTA tests.

Figure 15 and Table III show that the peak of tan δ slightly shifts to higher temperatures, when the clay content increases, reaching 48°C for the clay mass fraction of 10%. This growth is more pronounced compared to the one revealed by DTA measurements, which indicates that the use of DMTA seems more appropriate to evaluate the material glass transition temperature.

The peak amplitude of tan δ decreases with increasing clay fraction, as reported in the literature particularly in the case of intercalated nanocomposites based on polyamide matrix.[42] This result suggests that the damping behavior of material diminishes as the clay content rises. These two phenomena can be explained by the reduction of mobility for some macromolecular chains of PA12, intercalated and confined in clay galleries.[43] Moreover, the peak height reaches a maximum of about 0.1 that is the same value recorded by Gloaguen *et al.*[44] for PA6/montmorillonite nanocomposites. However, unlike the results obtained by these authors, the peak shape widens when the clay fraction increases for PA12/C30B nanocomposites.

CONCLUSION

The experimental work reported in this paper focused on the influence of the clay mass fraction on the structural, thermal, and dynamical mechanical properties of the PA12/C30B nanocomposites. In particular, SEM observations showed that the nanostructure coexists with a few micrometric aggregates, more numerous and larger as the clay fraction increases. Moreover,

The FTIR analysis highlighted that the organic modifier of clay is not degraded under chosen processing conditions, leading to the intercalated structure.

The DTA and TGA measurements showed that the thermal stability of the matrix PA12 is only slightly modified by adding clay. Nevertheless, the degradation starting temperature revealed the critical clay mass fraction of ~2%, beyond which nanocomposites are structured materials, in agreement with the results obtained by analyzing the melt-state rheological properties.[16]

A thorough study of viscoelastic properties of the PA12/C30B nanocomposites clearly highlights the reinforcing effect of clay particles. It was also shown that, like in melt-state, the extent of the linear behavior zone decreases in solid-state, as clay fraction increases. However, this decrease is more pronounced in melt-state. Indeed, the behavior nonlinearity is induced by the filler/filler and the matrix/filler interactions, but also partially governed by the matrix chain mobility which is obviously greater in melt-state than in solid-state.

Viscoelastic properties exhibit different frequency dependences in melt-state and in solid-state, partly due to the difference in matrix chain mobility that is easier in melt-state. However, they exhibit the same threshold fraction, ~2%, in both states, because they are strongly related to structural properties.

Finally, the temperature sweep tests highlight a reduction of chain mobility with increasing clay fraction.

ACKNOWLEDGMENTS

The authors thank Ludovic Teffo from the University of Brest and Emmanuel Penaud from the University of Tours for preparing PA12/C30B specimens used in DMTA tests.

REFERENCES

1. Ray, S. S.; Okamoto, M. *Prog. Polym. Sci.* **2003**, *28*, 1539.
2. Alexandre, M.; Dubois, P. *Mater. Sci. Eng.* **2000**, *28*, 1.
3. Usuki, A.; Hasegawa, N.; Kato, M. *Adv. Polym. Sci.* **2005**, *179*,135.
4. Kawasumi, M.; Hasegawa, N.; Kato, M.; Usuki, A.; Okada, A. *Macromolecules* **1997**, *30*, 6333.
5. Yuan, Q.; Awate, S.; Misra, R. D. K. *Eur. Polym. J.* **2006**, *42*, 1994.
6. Pandey, J. K.; Reddy, K. R.; Kumar, A. P.; Singh, R. P. *Polym. Degrad. Stab.* **2005**, *88*, 234.
7. Gilman, J. W. *Appl. Clay Sci.* **1999**, *15*, 31.
8. Sur, G. S.; Sun, H. L.; Lyu, S. G.; Mark, J. E. *Polymer* **2001**, *42*, 9783.
9. Médéric, P.; Aubry, T.; Razafinimaro, T. *Int. Polym. Proc.* **2009**, *24*, 261.
10. Dennis, H. R.; Hunter, D. L.; Chang, D.; Kim, S.; White, J. L.; Cho, J. W.; Paul, D. R. *Polymer* **2001**, *42*, 9513.
11. Usuki, A.; Kojima, Y; Kawasumi, M.; Okada, A.; Fukushima,Y.; Kurauchi, T.; Kamigaito, O. *J. Mater. Res.* **1993**, *8*, 1185.
12. Kojima, Y.; Usuki, A.; Kawasumi, M.; Okada, A.; Kurauchi, T.; Kamigaito, O.; Kaji, K. *J. Polym. Sci. Part B: Polym. Phys.* **1994**, *32*, 625.
13. Fornes, T. D.; Paul, D. R. *Macromolecules* **2004**, *37*, 7698.
14. Reichert, P.; Kressler, J.; Thoann, R.; Mulhaupt, R.; Stoppelmann, G. *Acta Polym.* **1998**, *49*, 116.
15. McNally, T.; Murphy, W.; Lew, C.; Turner, R. J.; Brennan, G. *Polymer* **2003**, *44*, 2761.
16. Aubry, T.; Razafinimaro, T.; Médéric, P. *J. Rheol.* **2005**, *49*, 425.
17. Aït Hocine, N.; Médéric, P.; Aubry, T. *Polym. Test.* **2008**, *27*, 330.
18. Médéric, P.; Razafinimaro, T.; Aubry, T. *Polym. Eng. Sci.* **2006**, *46*, 986.
19. Xie, W.; Gao, Z.; Pan, W. P.; Hunter, D.; Singh, A.; Vaia, R. *Chem. Mater.* **2001**, *13*, 2979.
20. Corcione, C. E.; Frigione, M. *Materials* **2012**, *5*, 2960.
21. Lionetto, F.; Maffezzoli, A. *Appl. Rheol.* **2009**, *19*, 1.
22. Talon, O. Amélioration de la résistance au choc du polyamide-12 par dispersion de polybutadiène. Etude des relations synthèse-structure-propriétés. PhD Thesis, INSA Rouen, **2002**.
23. Elf, Elf-Atochem, Rilsan® A: Step into the future, brochure, Elf Atochem SA, 1997.
24. Fornes, T. D.; Yoon, P. J.; Keskkula, H.; Paul, D. R. *Polymer* **2001**, *42*, 9929 [Erratum, Polymer 2002, 43, 2121].
25. Russell, J. D.; Farmer, V. C. *Clay Miner. Bull.* **1964**, *5*, 443.
26. Farmer, V. C. In The Infrared Spectra of Minerals; Farmer, V. C., Ed.; Mineralogy Society: London, **1974**; Chapter *15*, p 331.
27. Zhoua, L.; Chen, H.; Jiang, X.; Lu, F.; Zhou, Y.; Yin, W. *J. Colloid Interface Sci.* **2009**, *332*, 16.
28. Josh, G. V.; Patel, H. A.; Kevadiya, B. D.; Bajaj, H. C. *Appl. Clay Sci.* **2009**, *45*, 248.
29. Barbas, J. M.; Machado, A. V.; Covas, J. A. *Polym. Test.* **2012**, *31*, 527.
30. Yan, L.; Roth, C. B.; Low, P. F. *Langmuir* **1996**, *12*, 4421.
31. Cole, K. C. *Macromolecules* **2008**, *41*, 834.
32. Loo, L. S.; Gleason, K. K. *Macromolecules* **2003**, *36*, 2587.
33. Kashiwagi, T.; Harris, R. H.; Harris, J. R. *Polymer* **2004**, *45*, 881.
34. Dabrowski, F.; Bourbigot, S.; Delobe, R.; Bras, M. L. *Europ. Polym. J.* **2000**, *3*, 273.
35. Ogata, N.; Kawakage, S.; Ogihara, T. *J. Appl. Polym. Sci.* **1997**, *66*, 573.
36. Jimenez, G.; Ogata, N.; Kawai, H.; Ogihara, T. *J. Appl. Polym. Sci.* **1997**, *64*, 2211.
37. Chaou, S. Elaboration et caractérisation de nanocomposite à matrice polymère: approche expérimentale. PhD Thesis, Université Ferhat Abbas, Sétif, Algérie, **2010**.
38. Ghanbari, A.; Heuzey, M. C.; Carreau, P. J. *Polym. Int.* **2012**, *62*, 439.

39. Takayanagi, M.; Vemura, S.; Minami, S. *J. Polym. Sci. Part C: Polym. Symp.* **1964**, *5*, 113.
40. Ji, X. L.; Jing, J. K.; Jiang, W.; Jiang, B. Z. *Polym. Eng. Sci.* **2002**, *42*, 983.
41. Razafinimaro, T. Étude des relations structure-propriétés rhéologiques: mécaniques de nanocomposites polyamide12/argile organophile: effet de la fraction volumique et des conditions de mélangeage. PhD Thesis, Université de Bretagne Occidentale, Brest, 2006.
42. Chiu, F. C.; Lai, S. M.; Chen, Y. L.; Lee, T. H. *Polymer* **2005**, *46*, 11600.
43. Vaia, R. A.; Sauer, B. B.; Tse, O. K.; Giannelis, E. P. *J. Polym. Sci. Part B: Polym. Phys.* **1997**, *35*, 59.
44. Gloaguen, J. M.; Lefebvre, J. M. *Polymer* **2001**, *42*, 5841.